Computers and Concrete, *Vol. 13, No. 6 (2014) 781-798*
DOI: http://dx.doi.org/10.12989/cac.2014.13.6.781

Method for estimating workability of self-compacting concrete using mixing process images

Shuyang Li and Xuehui An*

State Key Laboratory of Hydro Science and Engineering, *Tsinghua University*, *100084-Beijing*, *China*

(*Received February 26, 2013, Revised April 22, 2014, Accepted April 24, 2014*)

Abstract. Estimating the workability of self-compacting concrete (SCC) is very important both in laboratories and on construction site. A method using visual information during the mixing process was proposed in this paper to estimate the workability of SCC. First, fourteen specimens of concrete were produced by a single-shaft mixer. A digital camera was used to record all the mixing processes. Second, employing the digital image processing, the visual information from mixing process images was extracted. The concrete pushed by the rotating blades forms two boundaries in the images. The shape of the upper boundary and the vertical distance between the upper and lower boundaries were used as two visual features. Thirdly, slump flow test and V-funnel test were carried out to estimate the workability of each SCC. Finally, the vertical distance between the upper and lower boundaries andthe shape of the upper boundary were used as indicators to estimate the workability of SCC. The vertical distance between the upper and lower boundaries was related to the slump flow, the shape of the upper boundary was related to the V-funnel flow time. Based on these relationships, the workability of SCC could be estimated using the mixing process images. This estimating method was verified by three more experiments. The experimental results indicate that the proposed method could be used to automatically estimate SCC workability.

Keywords: self-compacting concrete; workability; mixing process; digital image processing; slump flow test; V-funnel test

1. Introduction

Self-compacting concrete (SCC) was first developed in 1988 (Ozawa *et al*. 1989). It has high workability, which refers to the self-compact ability (Ferraris *et al*. 2000). Self-compact ability contains the high deformability and segregation resistance of fresh concrete. SCC workability determines whether a concrete is qualified for construction. Therefore, estimating SCC workability before placement is very significant.

Slump and V-funnel tests are the two most widely used tests in estimating SCC workability (Okamura and Ouchi 2003, Ferraris *et al*. 2000). Slump flow (*SF*) indicates the deformability of SCC, whereas V-funnel flow time (*VF*) indicates viscosity and segregation resistance ability. Therefore, these two tests are necessary for mix design in laboratories and for quality control on

*Corresponding author, Professor, E-mail: anxue@tsinghua.edu.cn

http://www.techno-press.org/?journal=cac&subpage=8 ISSN: 1598-8198 (Print), 1598-818X (Online)

construction sites. However, these tests present a number of problems in practice. One problem is that slump and V-funnel tests are always required before concrete placement to ensure that the SCC has good workability. Such requirement costs a large amount of labor and time. Another problem is that SCC workability can only be determined immediately before placement. When the concrete is not a qualified SCC, the mixture is wasted and engineers need to change the mix design.

The aforementioned issues can be addressed if SCC workability can be estimated during the mixing process. Cazacliu and Roquet (2009) showed that power consumption can be used to descri be the mixing process. This approach usually focuses on the homogenization of concrete. Chopin *et al*. (2007) indicated that a concrete mixer can be considered as a large rheometer. SCC rheological parameters can be obtained by considering fresh concrete as a Bingham material. Beaupré (1994) proposed a method that uses rheological parameters to estimate if a mixture is a qualified SCC. However, using a mixer as a reliable rheometer remains an open question (Chopin *et al*. 2007). A number of experienced engineers can estimate SCC workability by watching the mixing process. Thus, using digital image processing (DIP) to estimate SCC workability during the mixing process may be an effective solution. Cabaret *et al*. (2007) proposed a method of mixing-time analysis using image processing. This process determines mixing time by quantifying color evolution in a transparent stirring tank. Several studies used DIP to analyze aggregate settlements or cracks (Marinoni *et al*. 2005, Hutchinson and Chen 2006, Lee *et al*.2013); however only a few used DIP to study the concrete mixing process. Daumann and Nirschl (2008) used DIP to measure the mixing efficiency of solid mixtures which consist of particles with different sizes and colors. Based on this method, Daumann *et al*. (2009) used ultramarine blue as tracer component and determined the homogeneity of mixtures during concrete mixing process.

The purpose of this study is to provide a method for estimating SCC workability during the mixing process. Concrete mixing processes were recorded on video; and then the visual features of the mixing process were analyzed using DIP. The relationship between the visual features of the mixing process and SCC workability was further analyzed. Based on this relationship, a method for estimating SCC workability automatically was proposed.

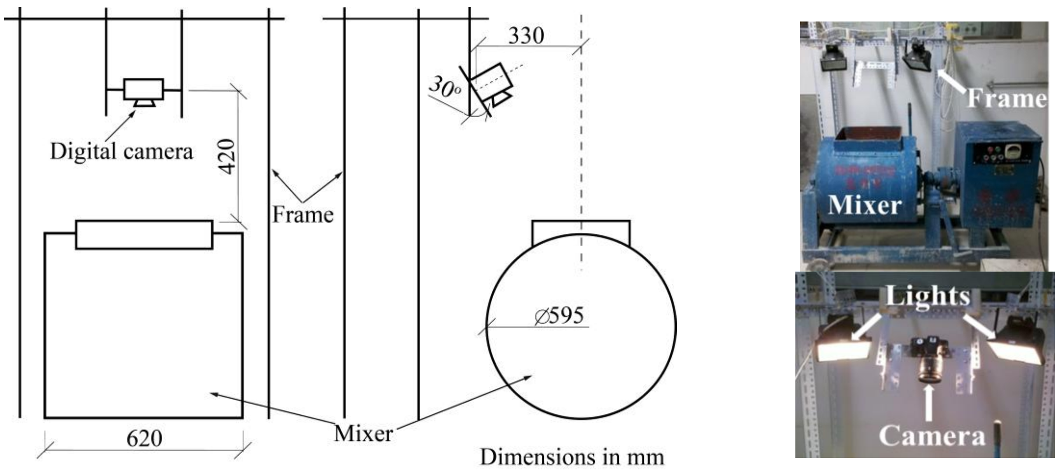

(a) Schematic diagram (b) Photographs

Fig. 1 Schematic diagramand photographs of the test setup

Fig. 2 The 60-liter, single-shaft mixer used in the experiments

2. Experimental study

2.1 Test setup

The experimental setup is shown in Fig. 1. The mixer used in all the tests was a 60-liter, single-shaft mixer (Fig. 2). The rotating speed of the mixer was set to 35 rpm. A steel frame was placed beside the mixer. A Canon 500D digital camera and luminaires were mounted on the frame. The focal length of the camera lens was 18 mm. Mixing time was set to 240s for each test. During the mixing process, the camera was used to capture a video through the opening hatch at a frame rate of 30 fps. The video was used to extract a series of images for further analysis. After mixing, *SF* and *VF* were conducted to verify the workability of the mixture.

2.2 Materials and test specimens

The cement used for all the experiments was PO 42.5. Coarse aggregates were crushed stones with particle sizes between 5 mm and 20 mm. Fine aggregates were quartz sand with a maximum particle size of 5 mm. Polycarboxy latesuper plasticizer were used as the water reducing agent in the experiments. SCC volume for each experiment was 30L. Fourteen experiments were carried out using different SCC. Mix designs and properties of the 14 specimens are shown in Table 1.

Different water-cement ratios (*W/C*) and different plasticizer dosages were used to obtain SCCs with different work abilities. The *W/C* values for each test are 0.8, 0.9, 1.0, 1.1 and 1.2, respectively. For the specimens with a same *W/C*, plasticizer dosages increased gradually. For example, specimens A1 to A4 have a same *W/C* of 1.0, and the plasticizer dosages increased from A1 to A4.

2.3 Test results

The *SF* and *VF* results of all the specimens are listed in the last two columns in Table 1. Different *W/C* values lead to different viscosities. In general, *VF* decreases with the increase of *W/C*. For a given *W/C* value, the plasticizer dosage was changed to obtain SCC with different deform abilities. For example, specimens A1, A2, A3 and A4 had the same *W/C* of 1.0.

Table 1 Mix design and SCC properties

Specimen	Water-cement ratio (Volume ratio)	Plasticizer (kg/m^3)	Cement (kg/m^3)	Water (kg/m^3)	Gravel (kg/m^3)	Sand (kg/m^3)	*SF* (mm)	*VF* (s)
A1	1.0	2.98	597	190	753	855	435	26.75
A2	1.0	4.18	597	189	753	855	690	15.31
A3	1.0	4.77	597	189	753	855	740	11.81
A4	1.0	8.95	597	185	753	855	805	60.15
B1	1.1	2.84	568	199	753	855	325	26.37
B2	1.1	3.98	568	198	753	855	670	10.52
B3	1.1	4.89	568	198	753	855	750	13.7
B4	1.1	5.68	568	197	753	855	755	22.06
C1	1.2	2.17	543	208	753	855	405	7.21
C2	1.2	2.98	543	208	753	855	680	5.63
C3	1.2	4.34	543	207	753	855	735	22.44
C4	1.2	5.43	543	206	753	855	770	36.65
D	0.8	7.96	663	167	753	885	735	96.03
E	0.9	4.40	628	179	753	885	435	76.53

The plasticizer dosages of these specimens were 2.98, 4.18, 4.77 and 8.95 kg/m^3, respectively; and their *SF* values were 435, 690, 740 and 805 mm, respectively. Thus, *SF* increases with the increase in plasticizer dosage. As a result, concrete specimens with different work abilities were obtained. Specimens A1, B1 and C1 have unqualified *SF* and *VF* caused by an insufficient deformability. Specimens A2, A3, B2, B3 and C2 are qualified SCC. Specimen D has an unqualified *VF* caused by a large viscosity. Specimen E has unqualified *SF* and *VF* because of large viscosities and insufficient deform abilities. Segregation occurred in specimens A4, B4, C3 and C4.

3. Methodology

3.1 Features extracted from mixing process images

Mixing process images include the entire mixing process. However, the image of interest is the moment when the blades move at the position where their left arm forms a 20° angle with the vertical immediately before the mixer stops. Fig. 3 is the image of interest of specimen A1. An image of interest has a resolution of 1280 pixels × 720 pixels. Later on in this study, image processing methodswillnot be applied on the entire image, but only on the region of interest (ROI). The white frame in Fig. 3 shows the position and size of the ROI.

The ROIs of the 14 specimens are shown in Fig. 4. In the different experiments, the SCCs on the blades form different shapes. The rotating blades push up the SCC. The shape of the mixture is supposed to be related to the workability of the concrete, which is consistent with experience. Therefore, using this shape to differentiate SCC workability in the mixer is possible. To describe this shape, its upper and lower boundaries are chosen as two features. The two boundaries are marked with white lines in Fig. 4, which are manually picked.

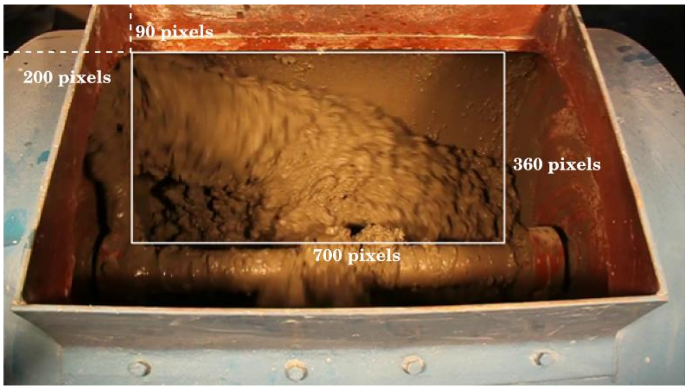

Fig. 3 The image of interest and its range of interest (ROI)

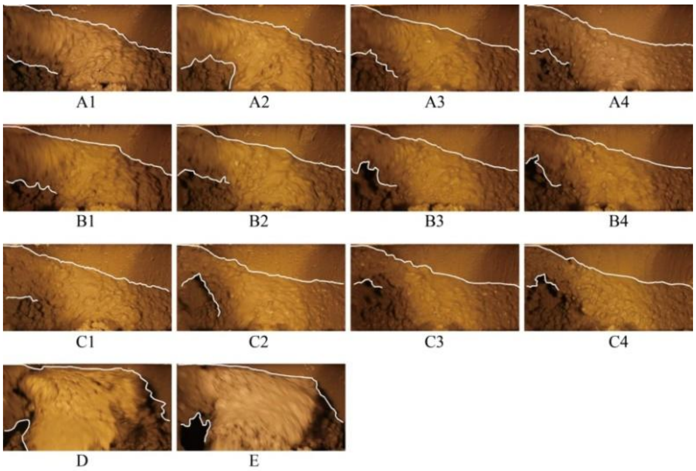

Fig. 4 The ranges of interest (ROIs) of all specimens

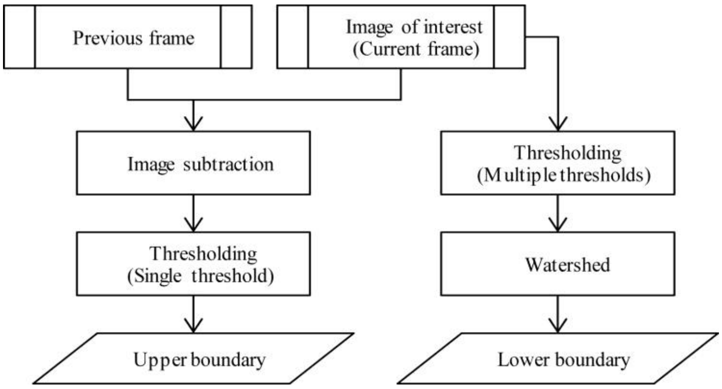

Fig. 5 Flowchart for detecting boundaries in a mixing image by digital image processing

3.2 Image processing

Determining the two boundaries in a mixing image necessitates separating the SCC region pushed upward by the rotating blades from the background. Several DIP methods can be used for image segmentation. Examples of such methods include edge detection (Carron and Lambert 1994), thresholding (Otsu 1979), region-based segmentation (Haddon and Boyce 1990), and watershed segmentation (Beucher 1992). In this study, image subtraction and thresholding methods were used to detect the upper boundary, whereas the watershed method was used to detect the lower boundary. The procedure for detecting boundaries of the mixing images via image processing is shown in Fig. 5. Taking specimen A2 as an example, the procedure is explained in detail in the following paragraphs.

3.2.1 Image subtraction

Mixing videos are continuous records of the mixing process. Given the aforementioned video frame rate of 30 fps, the camera captures animage every 0.33 s. Therefore, a frame is generated

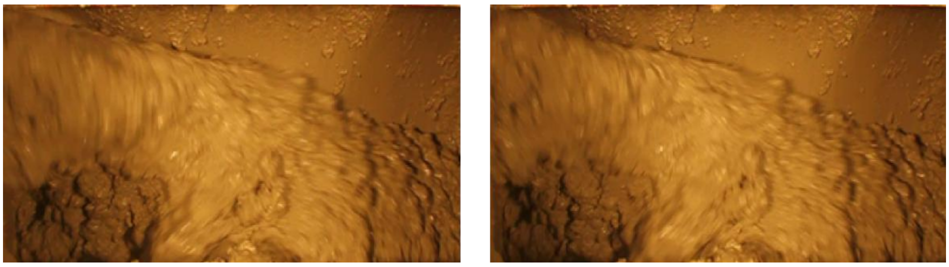

The current frame (image of interest) The previous frame

(a) The image of interest and its previous frame of Specimen A2

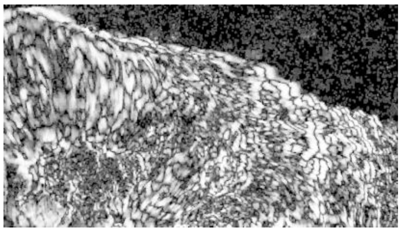

(b) Image subtraction between two neighbor frames (after histogram equalization)

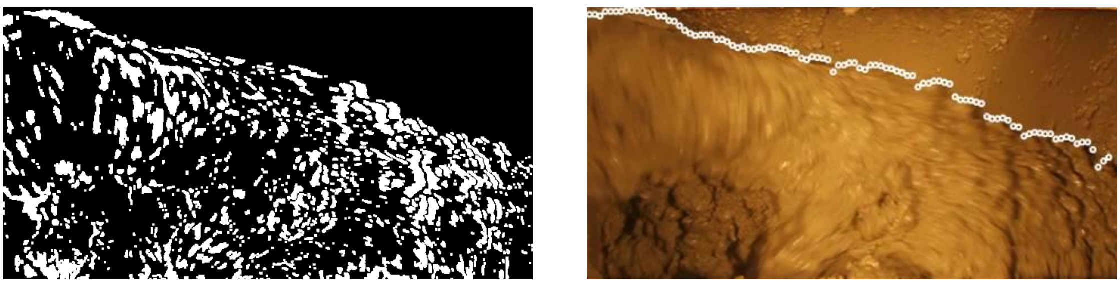

(c) Segmentation of Fig. 6(b) using Otsu’s method (d) Points on the upper boundary

Fig. 6 Image subtraction between neighbor frames of mixing images

0.33 s after its previous neighbor frame. During the period between two neighbor frames, the mixer wall remains still; by contrast, the blades and the SCC in the mixer rotate. Thus, the trunk shell of the mixer exhibits less change than the SCC in neighbor frames. The upper boundary is a dividing line between the mixer wall and the SCC. In other words, the upper boundary can be detected by filtering the changed parts between neighbor frames. Image subtraction is a common method for enhancing differences between two images. In this study, the subtraction between the image of interest and its previous frame was implemented to distinguish between larger changed region and smaller changed region. Atpoint (x, y), image differences are given by:

$$D(x, y) = f_c(x, y) - f_p(x, y) \tag{1}$$

where $f_c(x, y)$ is the intensity of the current frame, $f_p(x,y)$ represents the intensity of the previous frame, and $D(x,y)$ denotes differences between f_c and f_p.

Fig. 6(a) shows the image of interest and its previous frame of specimen A2. Their subtractionis presented in Fig. 6(b). The image is equalized for easy viewing. The intensity of the subtraction process indicate how different the two neighbor frames are. A particular section changes more when it is brighter. Therefore, sections with higher intensities are supposed to be SCC parts.

3.2.2 Optimum global Thresholding

After image subtraction, the brighter regions can already be distinguished. The upper boundary can be extracted from the image. Thresholding is widely used for image segmentation (Gonzalez and Woods 2010). The basic procedure for thresholding is as follows. First, a threshold is selected. Second, for any point (x,y) in the image, the resulting image of the thresholding, denoted as $g(x,y)$, is given by:

$$g(x, y) = \begin{cases} 1 & \text{if} \quad f(x, y) > T \\ 0 & \text{if} \quad f(x, y) \le T \end{cases} \tag{2}$$

where T denotes the threshold and $f(x,y)$ representsthe intensity of the input image. When threshold $T$is constant for the entire image, thresholding is called global thresholding. The effect of thresholding depends on a proper threshold.

Otsu (1979) proposed a method that automatically obtains the optimum global threshold using intensity histogram. The main basis of Otsu's method is using statistical theory to determine a threshold that divides the intensity histogram of the inputimage into two parts with the largest separability. Fig.6(c) demonstrates the application of Otsu's method on image subtraction between two neighbor frames (Fig. 6(b)). Fig. 6(c) is a binary image, wherein foreground pixels represent the region with larger changes. Therefore, the upper boundary can be determined by highlighting the top points of the foreground regions, as shown in Fig. 6(d).

3.2.3 Watershed segmentation

Watershed segmentation is an image segmentation method. A digital image has three dimensions: two spatial coordinates and intensity. Therefore, an image can be treated as a topographical map. Under such interpretation, a regional minimum (a dark region) indicates a basin, and a bright region indicates a crest. The lines between different basins and crests represent watershed lines, which automatically segment the given image. Marker-controlled watershed segmentation (Beucher 1992) is used to determine the lower boundary. In this processing technique, using the entire ROI is not necessary. Watershed segmentation was applied to a sub-image of the ROI, as shown in Fig. 7(a).

As shown in Fig. 7(a), the regions on either side of the lower boundary have distinctly different intensities. Therefore, bright and dark regions are two kinds of markers used in watershed segmentation. These markers can be selected using two thresholds. Otsu’s method can be extended to multiple thresholds because the separability measure can be extended to multiple classes (Fukunaga1972). Fig. 7(b) shows the markers generated using the extended Otsu’s method. The final watershed line, which approximates the lower boundary, is obtained, as shown in Fig. 7(c).

The comparison between boundaries picked manually and boundaries obtained using DIP is shown in Fig. 8. It shows that the DIP method can automatically extract the boundaries with a high accuracy.

3.3 Quantifying image features

As previously mentioned, the upper and lower boundaries are chosen as the features of mixing images. Quantitative indicators of the features are needed to compare different images. In this study, the shape of the upper boundary and the vertical distance between the upper boundary and the lower boundary were selected as the indicators for quantifying image features.

3.3.1 Average vertical distance between the upper and lower boundaries

The vertical distance between the upper and lower boundaries, denoted as H_a is given by:

$$H_a = \frac{A}{w} \tag{3}$$

where A is the area between the upper and lower boundaries and w represents the width along the horizontal direction of A. Fig. 9 shows a graphical explanation for H_a.

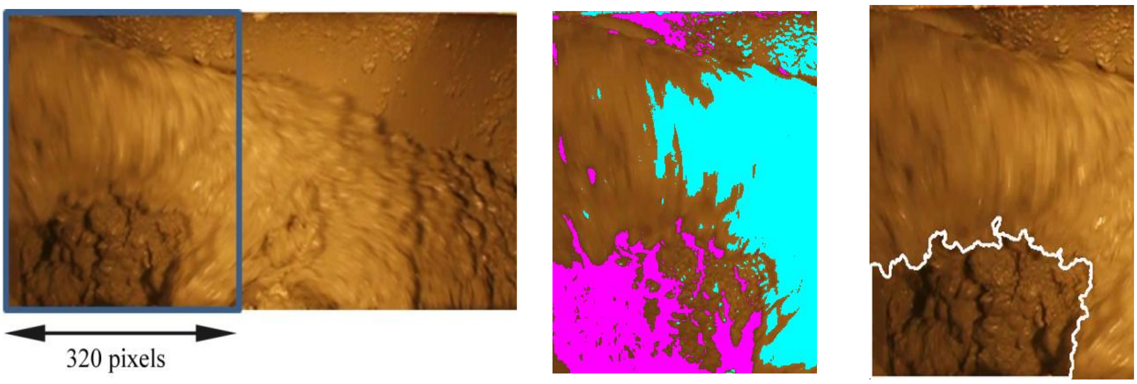

(a) A sub-region for watershed segmentation (b) Markers for watershed segmentation (c) Final watershed segmentation line

Fig. 7 Procedures and results of watershed segmentation

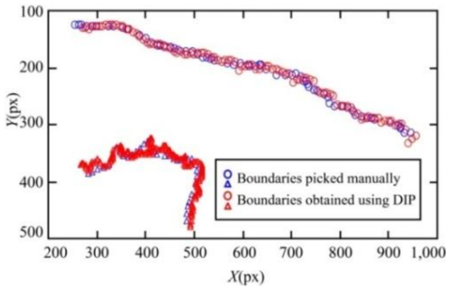

Fig. 8 Comparison between manually picked boundariesand boundaries obtained using DIP

3.3.2 Shape of the upper boundary

The method of describing the shape of the upper boundary in this paper is as follows: (1) to obtain the absolute positions of the points on the upper boundary; (2) to find the point on the upper boundary at which the upper boundary falls 25% along the vertical direction. The abscissa value of the point found in step (2) can be used as a quantitative indicator of describing the shape of the upper boundary.

The upper boundaries are three-dimensional (3-D) curves, for comparing these space curves, the absolute positions of the boundaries must be used. Three-dimensional reconstruction (Tang 2009) is commonly used to rebuild 3-D positions from a single image. The edge of the hatch of a mixer is rectangular, which can be used for camera calibration. The upper boundaries (the upper white lines in Fig. 4) are the intersecting lines between the concrete and the shell of the mixer. That is, the distance between any point on the upper boundary and the axis of the mixer is equal to the radius of the drum shell. Thus, the absolute position of the upper boundary in the 3-D space can be reconstructed. Fig. 10(a) illustrates this reconstruction concept.

For convenience of calculations, the positions of the points on the upper boundary are converted into plane coordinates. As shown in Fig. 10(a), the X-axis of the coordinates is along the axis of the mixer, the Y-axis of the coordinates is along the circumferential direction of the shell, and the origin is at the bottom of the mixer (point O in Fig. 10(a)). After 3-D reconstruction and conversion of the positions into plane coordinates, different upper boundaries are transformed into

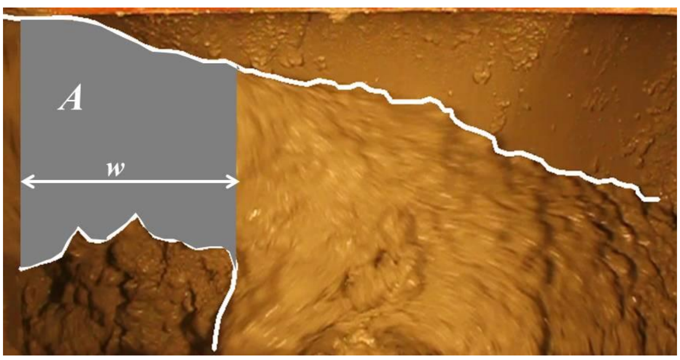

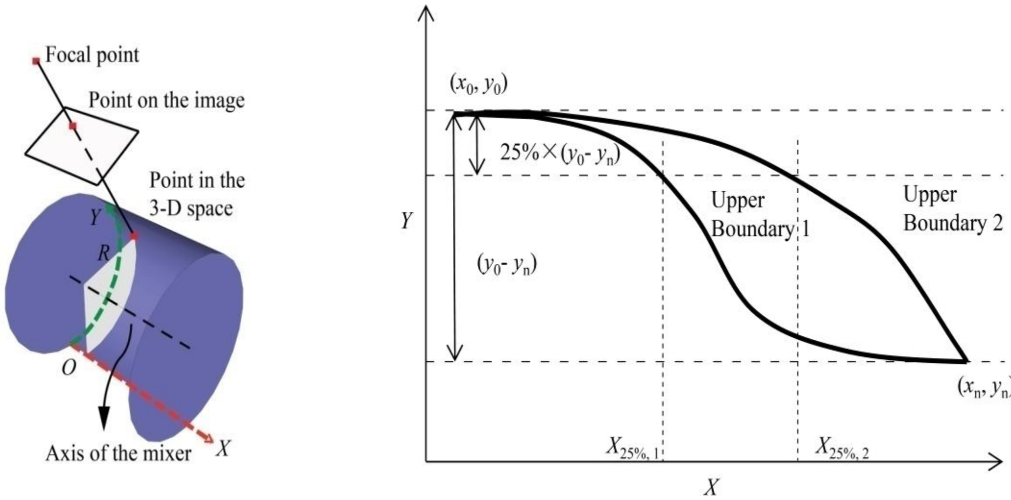

(a) The 3-D reconstruction of a point on the upper boundary (b) The calculation method of indicator for describing the shape of the upper boundary

Fig. 10 Method of describing the shape feature of the upper boundary

the same coordinate, and it is possible to compare the differences in shapes between different upper boundaries. Fig. 10(b) shows how to calculate the indicator of the upper boundary. Assuming that the first point on the upper boundary is (x_0, y_0), and the last point on the upper boundary is (x_n, y_n), find a point $P_{25\%}$ on the upper boundary which has an ordinate value equals to the result calculated by:

$$y_{25\%} = y_0 - 25\% \times (y_n - y_0) \tag{4}$$

where y_0 is the ordinate value of the first point on the upper boundary, y_n is the ordinate value of the last point on the upper boundary. Once the point $P_{25\%}$ is found, the abscissa value of $P_{25\%}$ (denoted as $X_{25\%}$) can be used as the indicator of the upper boundary's shape.

4. Results and discussion

4.1 Estimating method of SCC workability using mixing process images

4.1.1 Relationship between H_a and SF of SCC

Table 2 lists H_a calculated using Eq. (3) for specimens A1 to A4, B1 to B4 and C1 to C4.The relationship between H_a and *SF* is shown in Fig. 11. At a constant *W/C*, H_a is linearly related to *SF*. This relationship is expressed as:

$$H_a = k \cdot SF + 275 \tag{5}$$

where *SF* denotes the slump flow and *k* is the slope. A monotonic relationship is observed between *k* and *W/C*. Thus, interpolation and regression are appropriate methods for calculating the slope in practice. The following equation can be used to calculate k from W/C:

$$k = 0.288 - 0.3825 \cdot (W/C) \tag{6}$$

where W/C is the water-cement ratio.
Substituting Eq. (6) into Eq. (5) obtains the relationship between H_a and SF as:

$$SF = \frac{275 - H_a}{0.3825(W/C) - 0.288} \tag{7}$$

Eq. (7) can be used to calculate SF from H_a. Fig. 12 gives the comparison between the experimental SF and the calculated SF using Eq. (7). The relative errors between the experimental values and the calculated values are basically in the range of ±10%, except Specimen B1 that has an experimental SF of 325 mm and a calculated SF of 376 mm.

Table 2 SF and H_a for specimens A1~A4, B1~B4, C1~C4

Specimen	W/C	SF(mm)	H_a (pixels)
A1	1.0	435	235.6
A2	1.0	690	207.5
A3	1.0	740	203.3
A4	1.0	805	196.6
B1	1.1	325	225.1
B2	1.1	670	189.9
B3	1.1	750	181.4
B4	1.1	755	176.4
C1	1.2	405	206.9
C2	1.2	680	153.2
C3	1.2	735	150.2
C4	1.2	770	141.7

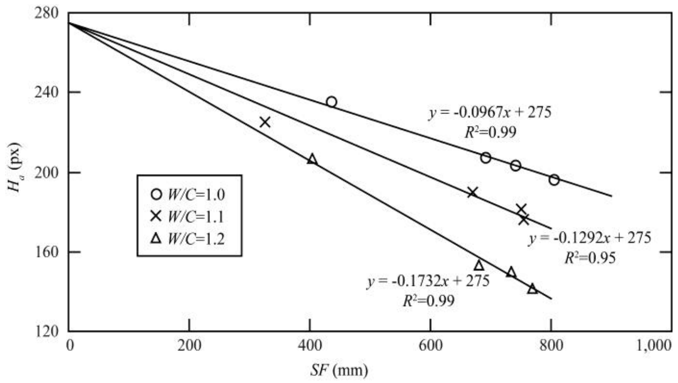

Fig. 11 Relationship between H_a and slump flow (SF) for 12 specimens

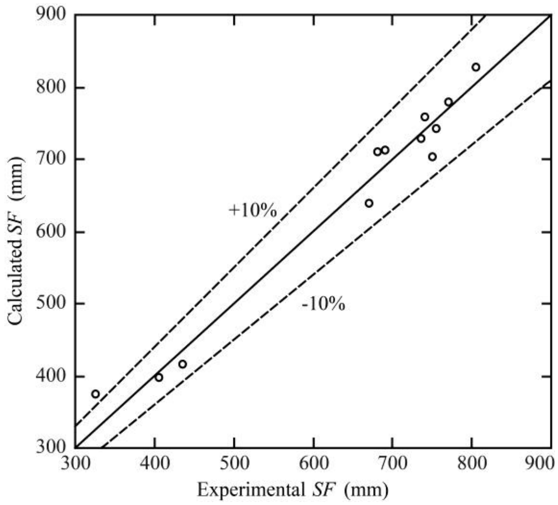

Fig. 12 Comparison between the experimental *SF* and the calculated *SF*

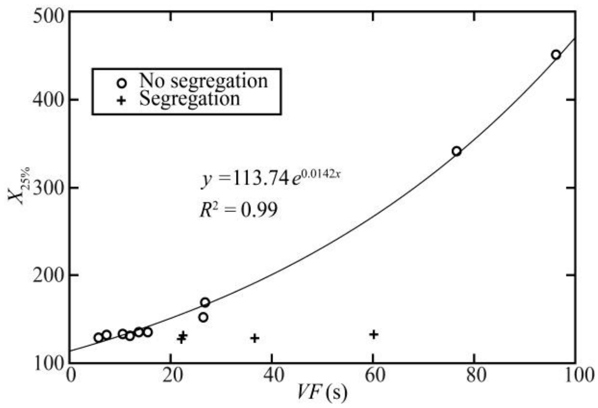

Fig. 13 Relationship between $X_{25\%}$ and V-funnel flow time (*VF*) for all specimens

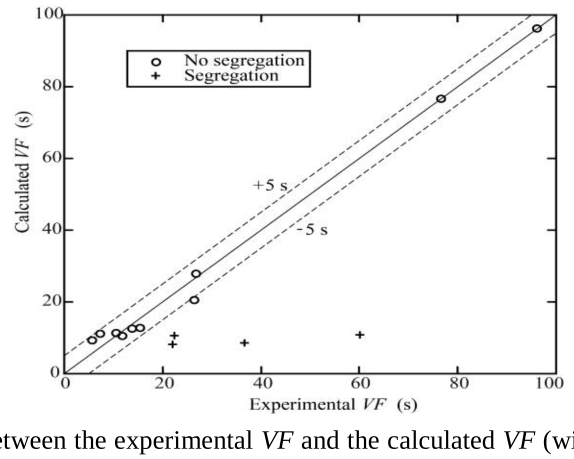

Fig. 14 Comparison between the experimental *VF* and the calculated *VF* (without consideration of segregation)

Table 3 *VF* and $X_{25\%}$ for all the fourteen specimens

Specimen	*W/C*	*VF* (s)	$X_{25\%}$ (mm)	Segregation occurred
A1	1.0	26.75	169.3	No
A2	1.0	15.31	136.3	No
A3	1.0	11.81	132.0	No
A4	1.0	60.15	132.3	Yes
B1	1.1	26.37	152.4	No
B2	1.1	10.52	133.7	No
B3	1.1	13.7	135.9	No
B4	1.1	22.06	127.6	Yes
C1	1.2	7.21	133.0	No
C2	1.2	5.63	129.6	No
C3	1.2	22.44	132.0	Yes
C4	1.2	36.65	128.2	Yes
D	0.8	96.03	451.6	No
E	0.9	76.53	341.2	No

Table 4 Mix design and SCC properties for further verification

Specimen	Water-cement ratio (Volume ratio)	Plasticizer (kg/m^3)	Cement (kg/m^3)	Water (kg/m^3)	Gravel (kg/m^3)	Sand (kg/m^3)	*SF* (mm)	*VF* (s)
T1	1.0	3.28	597	190	753	855	265	>60
T2	1.1	4.55	568	198	753	855	740	11.81
T3	1.1	4.83	568	198	753	855	810	57.75

Table 5 Estimating the workability of verification specimens based on mixing process images

Specimen	H_a	$X_{25\%}$	Experimental *SF* (mm)	Calculated *SF* (mm)	Experimental *VF* (s)	Calculated *VF* (s)
T1	255.6	324.3	265	205	>60	73.26
T2	180.9	132.8	740	709	11.81	11.03
T3	170.1	137.0	810	790	57.75	47.33

4.1.2 Relationship between H_a and SF of SCC

$X_{25\%}$ for all the specimens in Table 1 are listed in Table 3. At a constant W/C (for example, specimen A1 to A4, all these 4 specimens had the same *W/C* of 1.0), with the increase inplasticizer dosage, the *SF* increases, meanwhile the *VF* decreases firstly, and then increases. In other words, with the increase in *SF*, the *VF* decreases firstly, and then increases. This trend is consistent with the experimental results of Ozawa *et al* (1995). Khayat (1999) explained that the *VF* of SCC was influenced by two major factors: deformability and segregation resistance. With the increase in deformability, the viscosity and the segregation resistance decrease and this results the reducing of

VF. Further increase in deformability might lead to an increase in *VF*, since the concrete does not have enough cohesion to resist the segregation. Therefore, in this paper, the specimens are classified into two types: the specimens with and without segregation occurred, respectively.

The relationship between $X_{25\%}$ and *VF* is plotted in Fig. 13. In Fig. 13, the circle represents the specimen without segregation occurring, the cross represents the specimen with segregation occurring. The specimens without segregation can be well fitted using an exponential function:

$$X_{25\%} = 113.74e^{0.0142VF} \tag{8}$$

where *VF* is the V-funnel flow time of a specimen.

According to Eq. (8), *VF* of SCC can be calculated by $X_{25\%}$ as:

$$VF = 69.70\ln(X_{25\%}) - 329.72 \tag{9}$$

Fig. 14 gives the comparison between the experimental *VF* and the calculated *VF* using Eq. (9). For the specimens without segregation occurring, the absolute errors between the experimental values and the calculated values are basically in the range of ±5 s, except specimen B1 that has an experimental *VF* of 26.37 s and a calculated *VF* of 20.63s (see the circles in Fig. 14). For the specimens with segregation occurring (specimen A4, B4, C3 and C4), the experimental *VF* are 60.15 s, 22.06 s, 22.44 s and 36.65 s respectively, the calculated *VF* according to Eq. (9) are 10.77 s, 8.25 s, 10.61 s and 8.58 s (see the crosses in Fig. 14). Therefore, Eq. (9) is suitable for the specimens without segregation. However, when the segregation occurs, Eq. (9) cannot give the right *VF* value through $X_{25\%}$.

Eq. (9) cannot be used to estimate the *VF* of SCC with segregation. Therefore, a correction term should be introduced into Eq. (9) when SCC does not have enough segregation resistance. Since there is a trade-off between deformability and segregation resistance, it is possible to measure the extent of segregation by deformability indirectly. The *SF* is an indicator of deformability of SCC, and H_a has a connection with *SF*, therefore H_a might indicate the extent of segregation. Fig. 15 shows the relationship between *VF* and H_a.

From Fig. 15, we can see that for a given *W/C*, with the decrease of H_a, the *VF* decreases firstly, and then increases. The relationship between *VF* and H_a forms a U-shape curve. The decrease in H_a means the increase in *SF*, therefore Fig. 15 is another expression of the trade-off between deformability and segregation resistance. For a given *W/C*, when the H_a is smaller than a threshold value (H_T), there was a significant possibility of segregation, the segregation is probably more serious while the difference between H_a and H_T is larger. In practice, H_T can be obtained by interpolation or regression according to the experimental results. In this paper, according to the results in Fig. 15, the H_T was chosen as 203 px, 178 px and 152 px when the *W/C* was 1.0, 1.1, 1.2, respectively. And H_T can be calculated as:

$$H_T = 398 - 50(W/C)^2 - 145(W/C) \tag{10}$$

When H_a is smaller than H_T, Eq. (9) should be changed as:

$$VF = 69.70\ln(X_{25\%}) - 329.72 + \Delta \tag{11}$$

where Δ is the correction term for segregation.

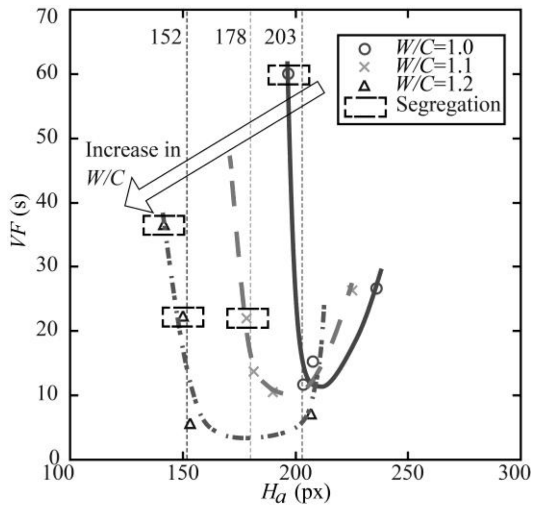

Fig. 15 Relationship between V-funnel flow time (VF) and H_a

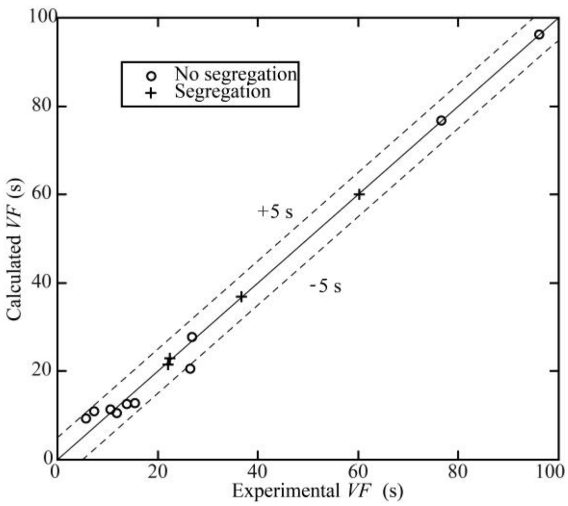

Fig. 16 Comparison between the experimental *VF* and the calculated *VF* (take segregation into consideration)

If H_a is smaller than H_T, *VF* would increase rapidly with the decrease of H_a. The correction term (Δ) was assumed having an exponential form. Considering *VF* increases with the increase in the difference between H_T and H_a, there should be a positive correlation between Δ and (H_T - H_a). In Fig. 15, the slope of the left part of the U-shape curve decreases with the increase in *W/C*, hence there should be a negative correlation between Δ and (*W/C*). In this paper, the correction termΔ was assumed in the form of:

$$\Delta = \alpha e^{\beta \frac{H_T - H_a}{(W/C)^{\gamma}}} \tag{12}$$

where α, β, γ are parameters fitted using experimental results and they should be updated with increase of experiment numbers.

Using the experimental results of the 14 specimens in Table 1, the parameters in Eq. (12) was obtained by regression:

$$\Delta = 10.307e^{0.2441\frac{H_T - H_a}{(W/C)^5}} \tag{13}$$

By introducing the correction term, Eq. (9) was transformed into:

$$VF = \begin{cases} 69.70\ln(X_{25\%}) - 329.72 & if \quad H_a \geq H_T \\ 69.70\ln(X_{25\%}) - 329.72 + \Delta & if \quad H_a < H_T \end{cases} \tag{14}$$

Fig. 16 gives the comparison between the experimental *VF* and the calculated *VF* using Eq. (14).Right results are given for the specimens with segregation occurring, the absolute errors between the experimental values and the calculated values are in the range of ±5 s (see the crosses in Fig 16).That shows Eq. (14) can be used to estimate the *VF* of SCC correctly.

4.2 Verification of the estimating method

For further verification, three more verificationtests were conducted. The mix designs of these specimens are shown in Table 4. Specimen T1 is unqualified because of its high viscosity, it was blocked while taking the V-funnel test; specimen T2 is qualified; and specimen T3 is segregated. The estimating method based on theDIP proposed in this paper was applied on these verification tests. The results are listed in Table 5. The results given by the proposed method show that specimen T1 had very limited deformability. Specimen T2 was qualified SCC. Although specimen T3 had good deformability, the SCC was segregated and it had a very long V-funnel flow time. The calculated results using DIP are consistent with the experimental results. Therefore, the workability estimating method based on mixing process images can give effective results automatically. It can be used to estimate the status of the SCC during the mixing process.

5. Conclusions

This paper presents a method for estimating SCC workability using visual information during the mixing process based on digital image processing. The mixing processes of 14 specimens produced by a single-shaft mixer were videotaped. The relationship between visual information and SCC workability was established by analyzing the videos of different SCCs' mixing processes. Image processing method was used to extract the features from the mixing videos automatically. Three more experiments were used to estimate and verify the relationship.We could conclude that:

- The appearance of the concrete mixture is related to its workability during the mixing process from the experiments.
- The two visual features, the shape of the mixture and the amount of the mixture carried on the mixer's blades, could be used to estimate the workability of concrete mixture in the mixing

process.

- Frame difference method was used to obtain the shape of the boundary between the mixture and the mixer, and the watershed segmentation was used to obtain the area of the mixture carried on mixer's blades in a mixing image.
- A method for estimating SCC workability automatically was proposed.The slump flow (SF) and the V-funnel flow time (VF) of SCC could be estimated effectively based on thevisual features of the mixture.

Based on this method, a real-time monitoring system can be developed to estimate SCC workability during the mixing process. It is an alternative of the slump flow and V-funnel tests. This kind of system might save time and labor both in laboratories and on construction sites.

Acknowledgements

This work is supported by State Key Laboratory of Hydro Science and Engineering (Grant No. 2012-Ky-02) and by the State Key Program of National Natural Science of China (Grant No. 51239006).

References

Beaupré, D. (1994), "Rheology of High Performance Shotcrete", Ph. D. Dissertation, Universityof British Columbia, Vancouver.

Beucher, S. (1992), "The watershed transformation applied to image segmentation", *Scanning Microsc. Suppl.*, **6**, 299-314.

Cabaret, F., Bonnot, S., Fradett, L. and Tanguy, P.A.(2007), "Mixing time analysis using colorimetric methods and image processing", *Ind. Eng. Chem. Res.*, **46**(14), 5032-5042.

Carron, T. and Lambert, P. (1994), "Color edge detector using jointly hue, saturation and intensity", *Proceedings of the IEEE International Conference on Image Processing*, Austin, USA, November.

Cazacliu, B. and Roquet, N. (2009), "Concrete mixing kinetics by means of power measurement", *Cement Concrete Res.*, **39**(3), 182-194.

Chopin, D., Cazacliu, B., de Larrard, F. and Schell, R. (2007), "Monitoring of concrete homogenisation with the power consumption curve", *Mater. Struct.*, **40**(9), 897-907.

Daumann, B., Anlauf, H. and Nirschl, H. (2009), "Determination of the energy consumption during the production of various concrete recipes", *Cement Concrete Res.*, **39**(7), 590-599.

Daumann, B. and Nirschl, H. (2008), "Assessment of the mixing efficiency of solid mixtures by means of image analysis", *Powder Technol.*, **182**(3), 415-423.

Ferraris, C.F., Brower, L., Ozyildirim, C. and Daczko, J. (2000), "Workability of self-compacting concrete", *Proceedings of the PCI/FHWA/FIB International Symposium on High Performance Concrete*, Orlando, USA, September.

Fukunaga, K. (1972), *Introduction to Statistical Pattern Recognition*, Academic Press, New York, NY, USA.

Gonzalez, R.C. and Woods, R.E. (2010), *Digital Image Processing*, Publishing House of Electronics Industry, Beijing, China.

Haddon, J.F. and Boyce, J.F. (1990), "Image segmentation by unifying region and boundary information", *IEEE Ttans. Pattern Anal. Mach. Intell.*, **12**(10), 929-948.

Hutchinson, T.C. and Chen, Z. (2006), "Improved image analysis for evaluating concrete damage", *J. Comput. Civil Eng.*, **20**(3), 210-216.

Khayat, K.H. (1999), “Workability, testing, and performance of self-consolidating concrete”, *ACI Mater. J.*, **96**(3), 346-353.

Lee, B.Y., Kim, Y.Y., Yi, S.T. and Kim, J.K. (2013), “Automated image processing technique for detecting and analysing concrete surface cracks”, *Struct. Infrastruct. Eng.*, **9**(6), 567-577.

Marinoni, N., Pavese, A., Foi, M. and Trombinoa, L. (2005), “Characterisation of mortar morphology in thin sections by digital image processing”, *Cement Concrete Res.*, **35**(8), 1613-1619.

Okamura, H. and Ouchi, M. (2003), “Self-Compacting Concrete”, *J. Adv. Concr. Technol.*, **1**(1), 5-15.

Otsu, N. (1979), “A threshold selection method from gray-level histograms”, *IEEE Trans. Syst. Man Cybern.*, **SMC-9**(1), 62-66.

Ozawa, K., Maekawa, K. and Okamura, H. (1989), “Development of high performance concrete”, *Proceedings of JCI*, **11**(1), 699-704. (in Japanese)

Ozawa, K., Sakata, N. and Okamura, H. (1995), “Evaluation of self-compact ability of fresh concrete using the funnel test”, *Concrete Library JSCE*, **25**, 59-75.

Tang, X. (2009), “Application of 3D virtual-reality and image modeling rebuilt technology in construction management system”, Bachelor Dissertation, Tsinghua University, Beijing. (in Chinese)

CC